FoMR
Frontiers of Multidisciplinary Research

Additive Manufacturing of Duplex Steel 2507 via Directed Energy Deposition: Process Optimization, Microstructure, and Mechanical Properties

Boyuan Li[a], Kangning Han[b], Junkai Cao[c], *Kun Zhou[d]

ABSTRACT

Duplex steels combine excellent mechanical properties and high corrosion resistance through a balanced ferrite-austenite microstructure, which is achieved by post heat treatment in traditional manufacturing. Metal additive manufacturing is a revolutionary manufacturing technique with high freedom of design, and it features a high cooling rate during the solidification of the melt pool, which makes it complex to obtain balanced ferrite and austenite phases. In this study, duplex steel 2507 was fabricated by laser-powder Directed Energy Deposition, and the phase constituent was tuned by powder flow rate at a constant laser power. A high powder flow rate yielded low energy density, suppressing the formation of ferrite and inducing lack-of-fusion pores, while a low flow rate enhanced the ferrite-austenite transformation due to higher energy density. An intermediate powder flow rate achieved a near-equal ferrite/austenite ratio, resulting in the best combination of strength and ductility. This work demonstrates a strategy for tailoring phase constituent in additively manufactured duplex steels and clarifies the process-microstructure-property relationship.

Received date: 05.11.2025
Accepted date: 01.12.2025

Keywords: Additive Manufacturing, Directed Energy Deposition, Duplex Steel, Microstructure, Phase Tailoring

https://doi.org/10.65601/FoMR.2026.1.1.2

[a]*Singapore Centre for 3D Printing, School of Mechanical and Aerospace Engineering, Nanyang Technological University, 50 Nanyang Avenue, Singapore 639798, Singapore, boyuan.li@ntu.edu.sg*

[b]*School of Mechanical and Aerospace Engineering, Nanyang Technological University, 50 Nanyang Avenue, Singapore 639798, Singapore N2309044A@e.ntu.edu.sg*

[c]*School of Mechanical and Aerospace Engineering, Nanyang Technological University, 50 Nanyang Avenue, Singapore 639798, Singapore junkai004@e.ntu.edu.sg*

***Corresponding Author:**

[d]*Singapore Centre for 3D Printing, School of Mechanical and Aerospace Engineering, Nanyang Technological University, 50 Nanyang Avenue, Singapore 639798, Singapore, kzhou@ntu.edu.sg*

INTRODUCTION

Duplex steels are promising structural materials owing to their excellent strength and corrosion resistance derived from balanced BCC ferrite (α) and FCC austenite (γ) phases (Fang et al., 2025. A near-equal ferrite/austenite fraction typically optimizes strength-ductility synergy and pitting resistance, whereas deviations from balance or the presence of deleterious secondary phases, such as Cr_2N and σ phase, can degrade performance (Francis & Byrne, 2021). Conventional manufacturing methods for duplex steels are casting and wrought, where post heat treatment is required to obtain the desired phase balance through controlled annealing (Han et al., 2023). However, it is challenging to fabricate complex geometries or functionally graded structures through traditional methods.

Additive manufacturing (AM) has emerged as a revolutionary technique which not only enables the capability to fabricate complex geometries, but also provides the feasibility to tailor phase constituents through process control (Li et al., 2021). Laser powder bed fusion (LPBF) is a popular metal AM method, where the metal powders are laid into a thin layer and selectively melt by a laser beam (Li et al., 2022). Zhao et. al., manufactured duplex steel 2205 by LPBF with optimized laser scanning speed to eliminate printing defects, but the printed part consisted of a majority of BCC phase with limited ductility (Zhao et al., 2023). Wang et. al., printed duplex steel 2205 by LPBF under varying volumetric energy density and elucidated the relationship between in-situ annealing and austenite formation during the melt pool solidification, and a FCC fraction of 6.6% was obtained by process optimization (G. Wang et al., 2025). Fang et. al., prepared the duplex steel 2205 reinforced by TiC through LPBF and achieved a refined grain size and embedded Ti-rich precipitates, but the printed part consisted of a high fraction of BCC phase where post heat treatment was applied to obtain the balance of FCC/BCC (Fang et al., 2023). Tao *et al.* printed an N-doped duplex steel powder by LPBF to unravel the thermodynamic evolution of ferrite/austenite duplex-phase, and established predictive phase fraction control for FCC phase (up to 44.9%) (Tao et al., 2025). Constrained by the high cooling rate of LPBF, it is challenging to fabricate duplex steels with balanced FCC/BCC ratio without post heat treatment and composition tailoring.

Directed Energy Deposition (DED) is another mainstream metal AM technique with moderate cooling rate, which is suitable for printing large parts owing to its advantages of high building rates and large building volume (Li et al., 2021). In addition, DED uniquely supports in-situ alloying, functional gradient structure, cladding, and repairing while enabling microstructure engineering through thermal history design. Salvetr *et al.* deposited duplex steel 2507 by DED, and the fraction of FCC phase was around 28% in the as-printed sample and improved to 50% by solution annealing at 1100°C for 60 min followed by water quenching (Salvetr et al., 2022). Wang *et al.* printed a duplex steel by laser-DED where the composition of Cr and Ni elements were modified, and a balanced ferrite/austenite duplex structure was obtained eliminating the need for subsequent heat treatment (Y. Wang et al., 2023). Jiang *et al.* printed duplex steel 2507 by DED with a near 50/50 ferrite-austenite phase ratio but the ductility of the printed part was low (15%) as compared to the cast counterpart (20%) which could be attributed to the inhomogeneous distribution of ferrite and austenite (Jiang et al., 2022). Wu *et al.* built an equal austenite/ferrite duplex structure with duplex steel 2205 by wire-arc DED by controlling the energy density and the composition of the shield gas, but the strength was still low and the mixture of shield gas increased the complexity of the printing process (Wu et al., 2024).

To fully release the potential of duplex steels in AM, it is necessary to develop economic and universal methods to control the phase constituent of AM-built duplex steel without introducing harmful secondary phase or changing the original composition.

In this study, duplex steel 2507 was printed by laser-powder DED under different powder flow rates. The densification of printed samples and the embedded defect were inspected. The microstructure was characterized systematically including the phase constituents, grain orientation, and elemental segregation. The mechanical properties of the printed parts were evaluated by tensile test. Effects of the powder flow rate and the intrinsic high cooling rate of DED on the densification, phase constituents, and mechanical properties were revealed. This study imparts substantial insights into the microstructure tailoring of duplex steels via DED.

METHODS

Material Characteristics

A spherical duplex steel 2507 powder fabricated by gas atomization (Sandvik AB, Sweden) was used as the feedstock for the laser-powder DED process (Fig. 1a). The powder exhibited a particle size distribution of 1–53 µm, and the D_{10}, D_{50}, and D_{90} values of the powder particle were 23.26, 30.24, and 46.16 µm, respectively (Fig. 1b). The duplex steel powder displayed a homogeneous distribution of the alloying elements such as Fe, Cr, Ni, and Mo obtained by energy dispersive spectroscopy (EDS) technique (Fig. 1c).

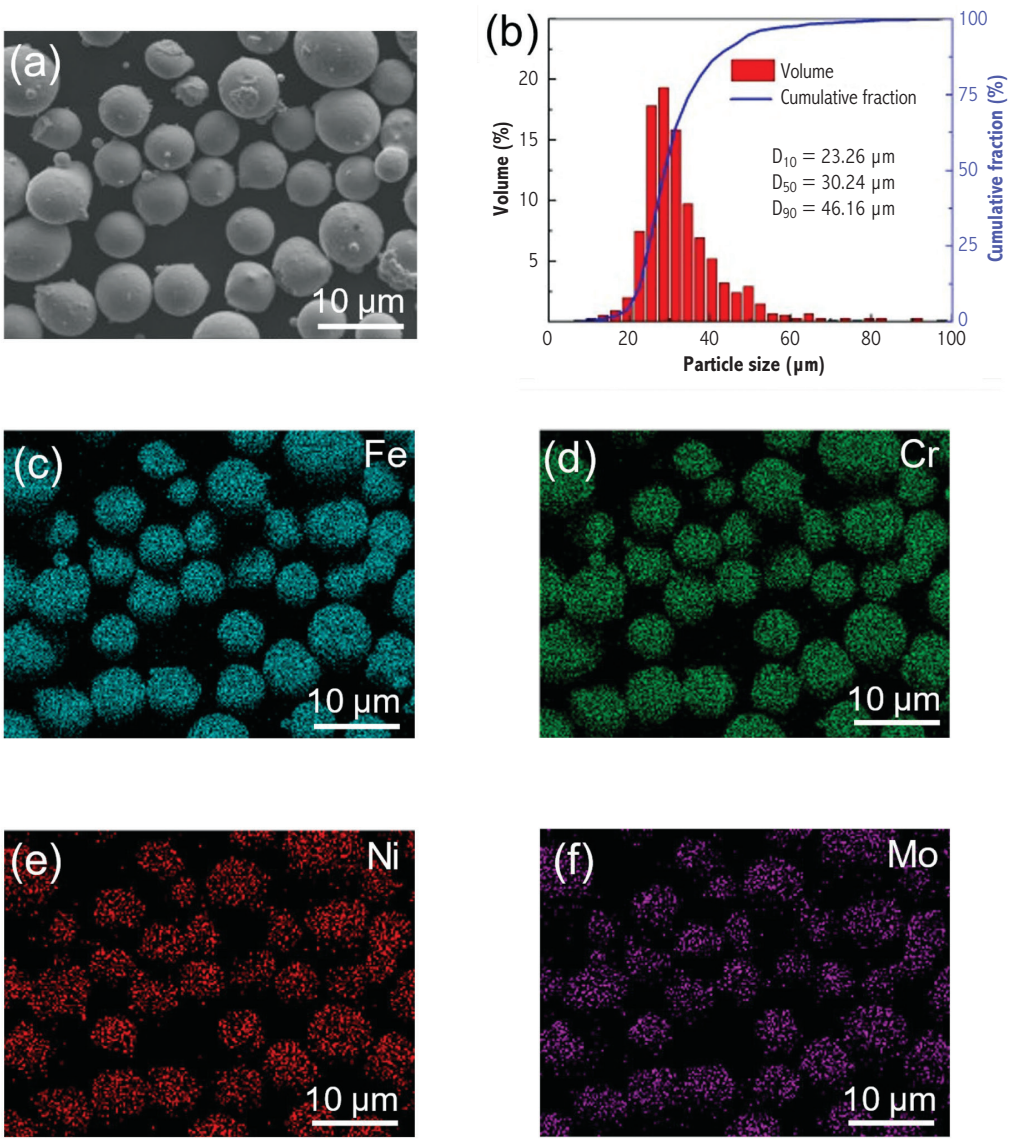

Figure 1 Characteristics of the duplex steel 2507 powder: (a) morphology, (b) particle size distribution, and (c–f) EDS mapping of Fe, Cr, Ni, and Mo elements, respectively.

Sample Preparation

A laser-powder DED printer (TruLaser Cell 3000, Trumpf Corp., Germany) was used to prepare the duplex steel 2507 sample as shown in Fig. 2a. Block-shaped samples were printed with dimensions of 15 × 15 × 45 mm^3. The specific printing parameters were detailed in Table 1, where different powder flow rates were applied, while other parameters were kept consistent. Fig. 2b indicated the dimension and orientation of the tensile specimen, which was extracted from the center of the block sample via electrical discharging machining (EDM, Troop-50, Troop Corp., China). Microstructure characterization was conducted for the region (green box in Fig. 2b) next to the gauge center of the tensile specimen.

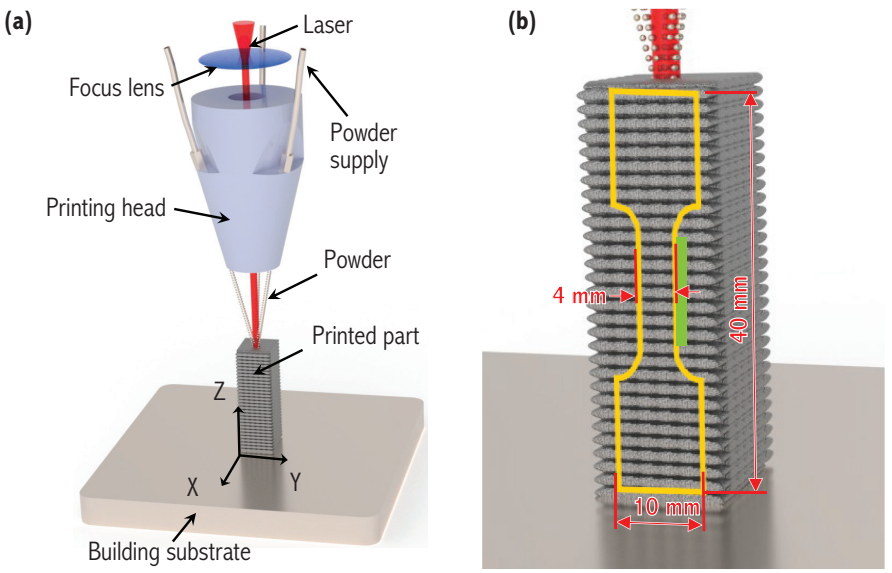

Figure 2 (a) Schematic of the laser-powder DED process and (b) the specification of tensile samples.

Table 1 Printing parameters for the laser-powder DED of duplex steel 2507.

Parameter	Value
Laser power	1000 W
Laser spot diameter	2 mm
Hatch space	2 mm
Hatch angle	90°
Powder flow rate	20.5, 25.1, 30.5, and 36.1 g/min
Carrier gas flow rate	4 L/min
Central gas flow rate	10 L/min

Characterization

A confocal microscope (LEXT OLS4000, OLYMPUS Corp., Japan) was employed to inspect the densification of the printed sample. An XRD (Bruker D8 Advance, Bruker Corp., U.S.) with a CuK_α radiation was utilized for phase identification. XRD scanning was conducted with a 2θ range, step size, scanning speed, generator voltage, and generator current of 30–100°, 0.01°, 0.135°·s^{-1}, 40 kV, and 25 mA, respectively. A field emission scanning electron microscope (FESEM, JEOL JSM 7800F, JEOL Corp., Japan) equipped with an EDS probe and electron backscatter diffraction (EBSD) detector was utilized to characterize the microstructure at the top, middle, and bottom locations. Secondary electron and backscatter electron imaging (BEI) modes were applied. EBSD data was analyzed in the AZtecCrystal software.

Mechanical Testing

The tensile samples were cut into a dog-bone shape with dimensions of 40 × 10 × 2 mm^3 and tested on a universal tensile machine (Shimadzu AGS-X, Shimadzu Corp., Japan). The strain rate was set at 0.01 min^{-1} and measured using a video extensometer. The mean values and deviation of yield strength (YS), ultimate tensile strength (UTS), and elongation were obtained from six samples. The fractography images of the tensile samples were obtained using FESEM.

RESULTS AND DISCUSSION

Microstructure

The microstructure of the DED-printed duplex steel 2507 is significantly affected by the powder flow rate. Different powder flow rates resulted in different volume energy density which directly led to various densification as shown in Fig 3. The low powder flow rate allowed the particles to be fully melt without causing key holes, while some gas pores were observed in Fig. 3a–c. As the powder flow rate increased, the energy density was reduced. Excessive particles were injected into the melt pool, and more laser energy was absorbed by the flying particles. The melt pool size was reduced under low energy density leading to the formation of lack-of-fusion pores between the adjacent tracks. The decreased energy density also enhanced the cooling rate of the melt pool and thus limited the liquid supply during the deposition process (Li et al., 2021).

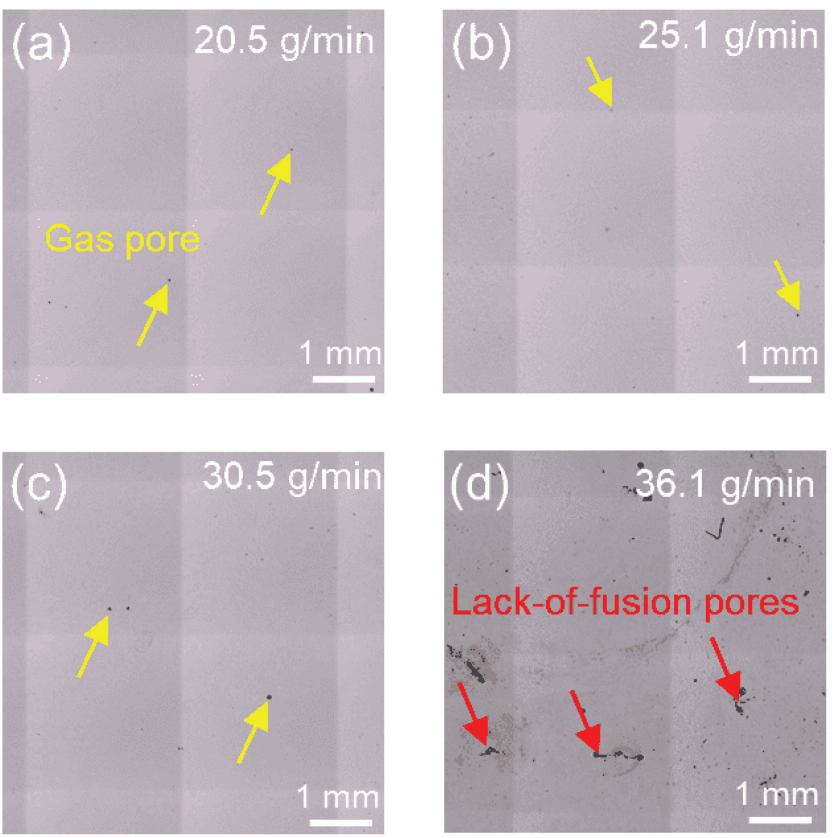

Figure 3 Optical microscope images showing the densification of the DED-printed duplex steel parts under different powder flow rates: (a) 20.5 g/min, (b) 25.1 g/min, (c) 30.5 g/min, and (d) 36.1 g/min.

The XRD patterns of the DED-printed duplex steel parts are shown in Fig. 4, which indicates the printed alloy consisting of FCC and BCC phases. The lattice parameters of FCC and BCC phases were 3.598±0.002 and 2.866±0.001 Å, respectively, which were consistent with previous reports (Salvetr et al., 2022). As the powder flow rate increased, the intensity of the FCC peak (111) decreased, which forecasted the fraction of FCC decrease. It was also noticed that the FCC peak (111) and BCC peak (110) shifted to the low angle direction as the powder flow rate increased corresponding to the increased interplane crystal spacing (zoom-in plots in Fig. 4). A higher powder flow rate can lead to

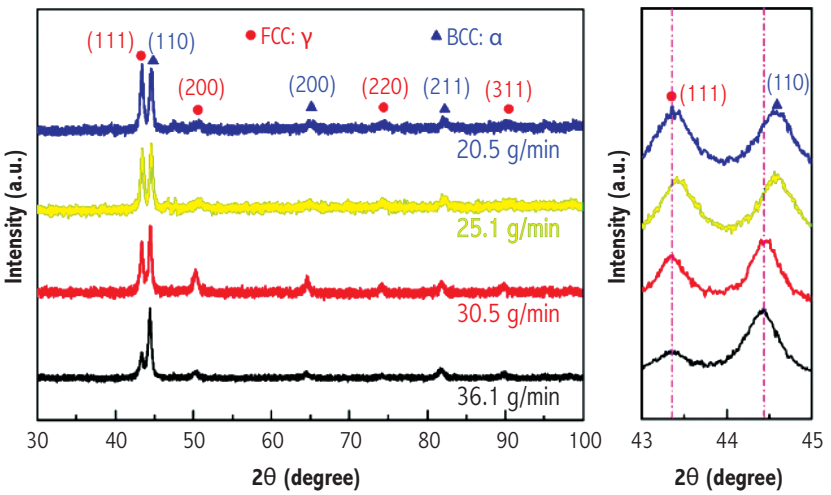

Figure 4 XRD patterns showing the phase constituents of the DED-printed duplex steel parts under different powder flow rates.

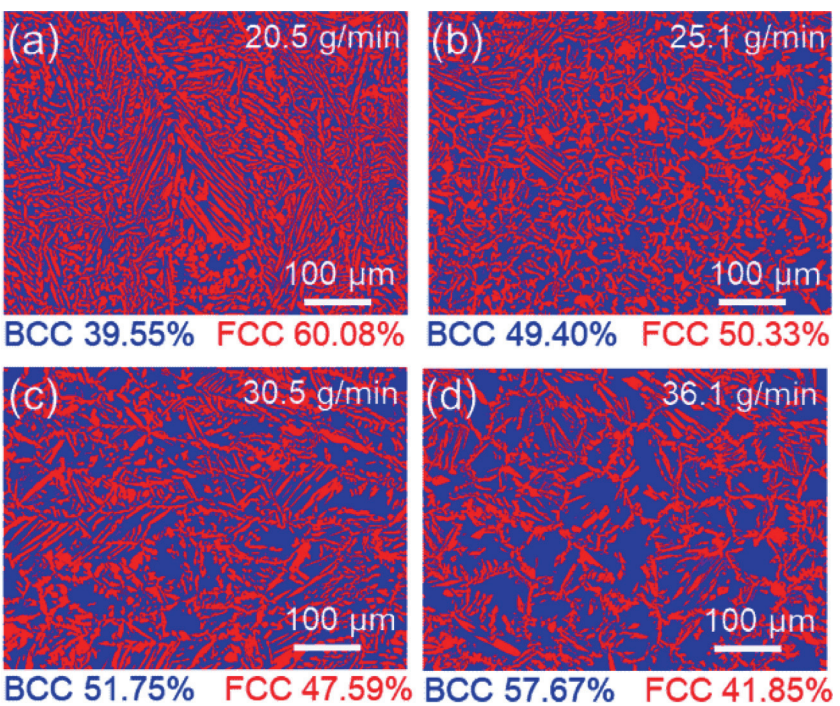

Figure 5 Phase distribution mapping of the DED-printed duplex steel parts under different powder flow rates: (a) 20.5 g/min, (b) 25.1 g/min, (c) 30.5 g/min, and (d) 36.1 g/min.

a higher cooling rate under consistent laser power. The high cooling rate can induce strong tensile residual stress in the printed part, and the crystal lattice tends to expand under the tensile stress (Liu et al., 2023).

The phase distribution mapping of the DED-printed duplex steel parts is shown in Fig. 5. The low powder flow rate of 20.5 g/min led to a high energy density and a low cooling rate, and thus more FCC phase (60.08%) was formed from the parent BCC phase (39.55% left) as shown in Fig. 5a. As the powder flow rate increased to 25.1 g/min, a near balance FCC/BCC ratio was achieved (Fig. 5b), which was desired for the duplex steel. The fraction of FCC phase decreased slightly when a powder flow rate of 30.5 g/min was used (Fig. 5c). The excessive powder flow rate of 36.1 g/min led to a low energy density and high cooling rate which limited the ferrite-to-martensite transition during the fast cooling process, thus the fraction of FCC phase dropped to 41.85% (Fig. 5d).

The elemental distribution of the DED-printed duplex steel parts with a powder flow rate of 25.1 g/min is shown in Fig. 6 which reveals the elemental segregation between FCC and BCC phase and the formation of secondary phase. Plate-like FCC (red arrow in Fig. 6a) austenite was embedded in the BCC ferrite matrix, and some nanoscale precipitates

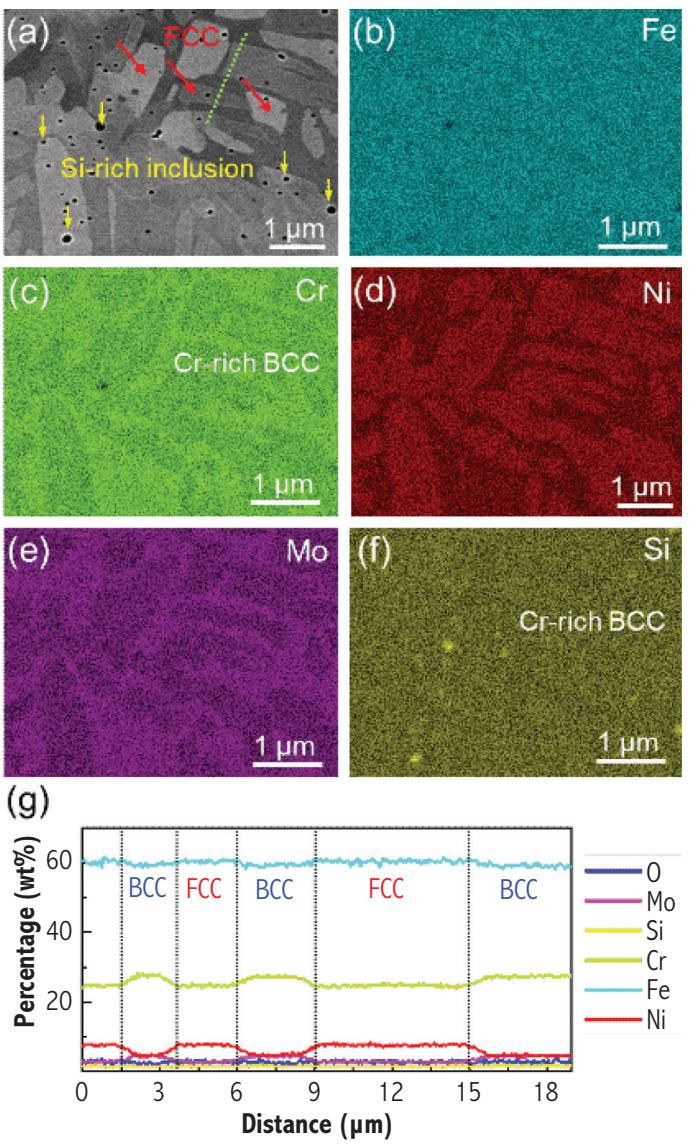

Figure 6 Elemental distribution of the DED-printed duplex steel parts with a powder flow rate of 25.1 g/min: (a) BEI image, (c–f) EDS mapping of Fe, Cr, Ni, Mo, and Si elements, respectively, and (g) EDS line scanning plots.

were observed located in the FCC phase or FCC/BCC boundaries. Fe element was distributed homogenously in FCC and BCC phases (Fig. 6b). However, Cr and Mo elements were enriched in the BCC matrix as shown in Fig. 6c and e, while Ni element was enriched in the FCC plates (Fig. 6d). The nanoscale precipitates were found to be Cr-rich inclusion which could have resulted from the oxidation of Si element during printing process as shown in Fig. 6f (Tao et al., 2025). The specific elemental partition between FCC and BCC phases was analyzed by EDS line scanning along the green line shown in Fig. 6a. The high cooling rate of DED suppressed the atom diffusion during ferrite-martensite transformation, and supersaturation solid solution matrix with element segregation between FCC and BCC was kept during the melt pool solidification as shown in Fig. 6g (Bajaj et al., 2020).

The crystal orientation of the DED-printed duplex steel parts with a powder flow rate of 25.1 g/min is shown in Fig. 7. The band contrast (BC) + phase distribution (PD) mapping showed a near equiaxed grain structure without pronounced columnar growth (Fig. 7a). Inverse pole figure (IPF) mappings displayed near random texture, and no preferred orientation was observed (Fig. 7b–d). Both BCC and FCC IPFs indicated near-random distribution of crystal orientation with modest maxima (1.47–1.69), and only faint <001> components were observed in the FCC IPF along the building direction (Fig. 7e and f). The minimally preferred orientation in both phases was expected to impart isotropic mechanical responses.

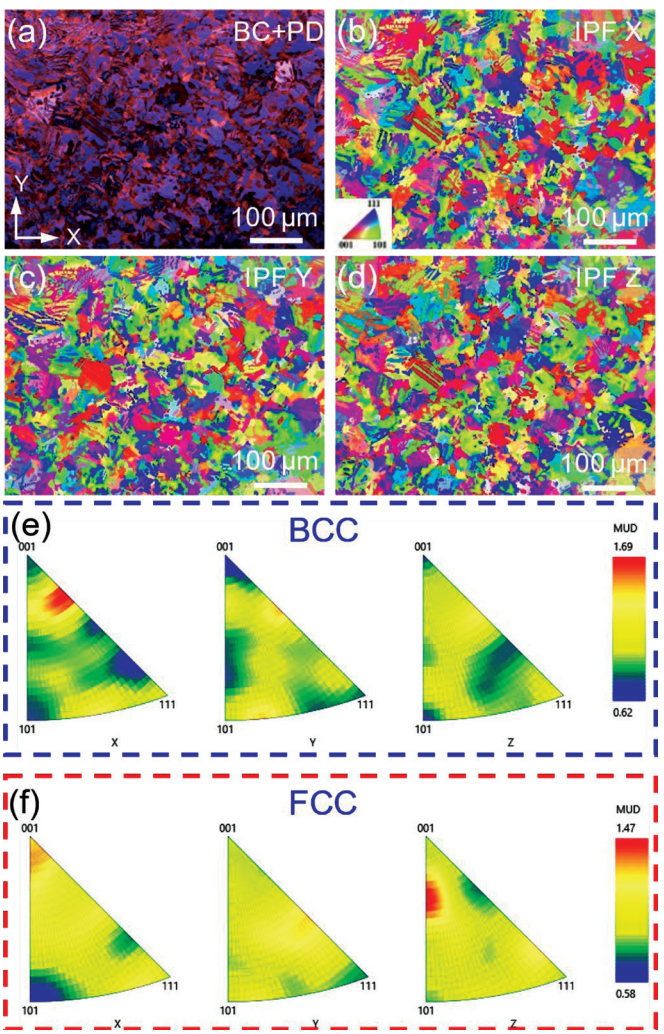

Figure 7 Crystal orientation of the DED-printed duplex steel sample with a powder flow rate of 25.1 g/min: (a) BC+PD mapping, (b) IPF X mapping, (c) IPF Y mapping, (d) IPF Z mapping, (e) IPF of the BCC phase, and (f) IPF of the FCC phase.

Mechanical Properties

The tensile properties of the DED-printed duplex steel parts are shown in Fig. 8. The duplex samples with high powder flow rate (36.1 g/min) failed early at a low strain of 1.41% due to the stress concentration at lack-of-fusion defects. The duplex steel samples printed with powder flow rates of 20.5, 25.1, and 30.5 g/min all exhibited a combination of high strength and good ductility (Fig. 8a). Among them, the sample printed with powder flow rate of 25.1 g/min with equal fractions of FCC and BCC displayed the best synthesized tensile properties, where a YS of 569.43 MPa, a UTS of 799.39 MPa, and an elongation of 36.03% were obtained. The specific values of tensile properties are given in Table 2. The printed duplex steel samples exhibited a notable work hardening during deformation which enabled uniform elongation and better strength-ductility synergy (Fig. 8b). As the deformation progressed, FCC phase suffered plastic deformation first, and misorientation was generated between FCC and BCC phases as shown in the kernel average misorientation (KAM)+PD mapping in Fig. 8c. Geometrically necessary dislocations (GNDs) were generated in the FCC+BCC matrix to maintain uniform distribution (Fig. 8d) (Chen et al., 2024). The balanced FCC/BCC structure was equipped with the highest phase boundary density which could promote the load sharing and maintain a high work hardening rate over a wide strain range.

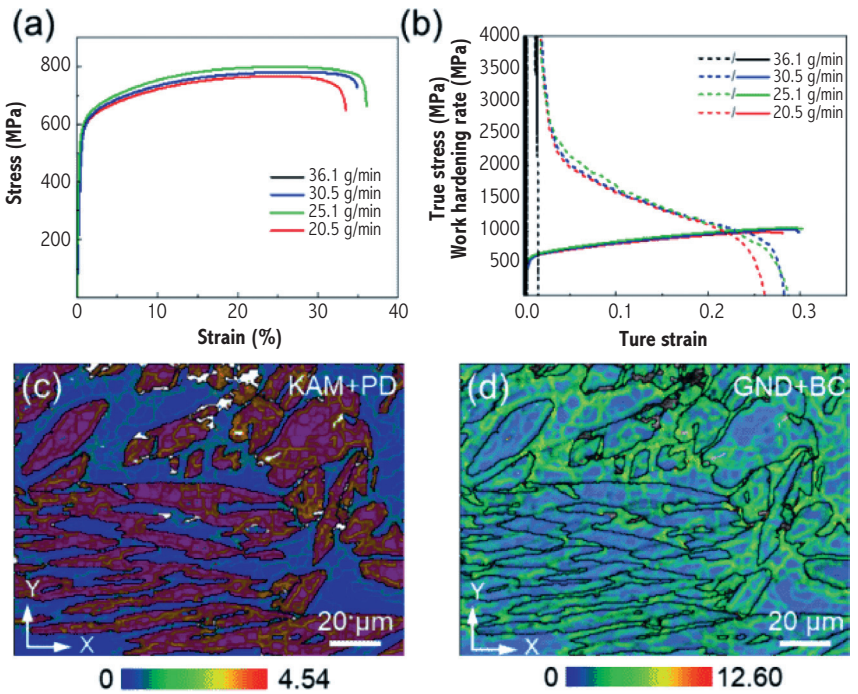

Figure 8 Tensile properties and deformed microstructure of the DED-printed duplex steel parts under different powder flow rates: (a) engineering stress–strain curves, (b) true stress–strain curves with corresponding work hardening rate curves, (c) KAM+PD mapping, and (d) GND+BC mapping.

Table 2 Tensile properties of the printed duplex steel samples.

Sample	YS (MPa)	UTS (MPa)	Elongation (%)
20.5 g/min	558.72±10.26	768.86±16.74	33.41±3.25
25.1 g/min	569.43±15.72	799.39±13.64	36.03±5.67
30.5 g/min	544.99±19.47	781.32±25.78	34.96±6.34
36.1 g/min	556.19±27.37	622.08±46.86	1.51±2.12

The fractography images of the tensile specimen (25.1 g/min) are shown in Fig. 9. The fracture surface exhibited a mixture of brittle and ductile fracture features. Equiaxed dimples interspersed with cleavage facets and tear ridges, evidencing local constraint and phase-dependent cracking. Cleavage facets surrounded by tear ridges were overserved on the fracture surface corresponding to the brittle BCC region (Fig. 9a). The higher-magnification view revealed dimples with Si-rich inclusions embedded inside, indicating inclusion-assisted void nucleation and growth followed by micro void coalescence (Fig. 9b). The coexistence of cleavage facets and ductile dimples points to heterogeneous plasticity and stress partitioning between ferrite and austenite with Si-rich inclusions acting as stress concentrators that degrade ductility.

cooling rate, and the ferrite-martensite transformation was suppressed resulting in a reduced fraction of FCC phase in the printed sample.

Elemental partition was induced between the FCC and BCC phases with Si-rich inclusions embedded in the FCC phase and FCC/BCC interfaces. The atom diffusion was suppressed under the high cooling rate, and thus the Ni enrichment was kept in the FCC phase while Cr and Mo enrichment was maintained in the BCC phase. Si element suffered oxidization during the printing process and resulted in the formation of Si-rich inclusions.

The balance FCC/BCC phases contributed to a high density of phase boundaries which imparted a strong work hardening by the back stress and

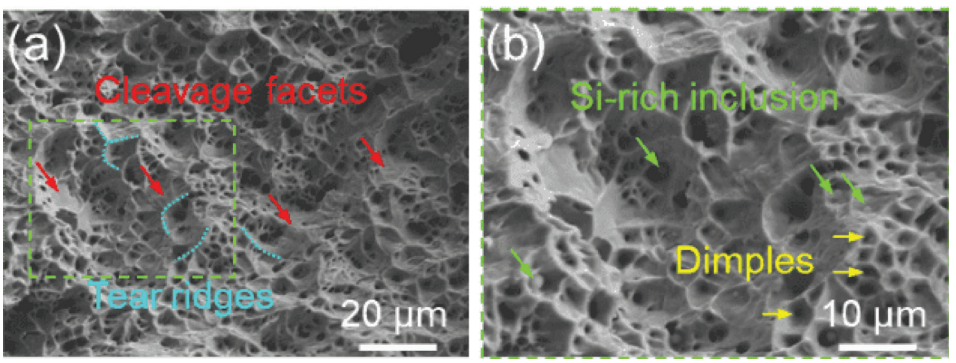

Figure 9 Fractography of the DED-printed duplex steel part with a powder flow rate of 25.1 g/min: (a) cleavage facets and tear ridges; (b) dimples and Si-rich inclusion.

CONCLUSION

The present study printed the duplex steel 2507 via laser-powder directed energy deposition under different powder flow rates. Effects of powder flow rates on the densification, microstructure, and mechanical properties were analyzed comprehensively. The main findings are summarized below.

The powder flow rate affected the energy density where an excessive powder flow rate led to the lack-of-fusion defects in the printed part. The defect caused the early failure of the printed tensile specimen due to stress concentration.

The powder flow rate tuned the fractions of FCC and BCC phases by influencing the cooling rate of the melt pool. As the powder flow rate increased, the reduced energy density induced an enhanced GNDs in the matrix. The substantial work hardening enabled uniform deformation and postponed the necking, thus achieving a synergy of high strength and good ductility in the printed part.

ACKNOWLEDGEMENT

This work was supported by the National Research Foundation, Prime Minister's Office, Singapore, under its Medium-Sized Centre funding.

Conflict of interest

The authors declare that they have no known competing financial interests or personal relationships that could have influenced the work reported in this paper.

Data availability

Data will be made available on request.

REFERENCES

Bajaj, P., Hariharan, A., Kini, A., Kürnsteiner, P., Raabe, D., & Jägle, E. A. (2020). Steels in additive manufacturing: A review of their microstructure and properties. *Materials Science and Engineering A*, *772*(October 2019). https://doi.org/10.1016/j.msea.2019.138633

Chen, H., He, Y., Dash, S. S., & Zou, Y. (2024). Additive manufacturing of metals and alloys to achieve heterogeneous microstructures for exceptional mechanical properties. *Materials Research Letters*, *12*(3), 149–171. https://doi.org/10.1080/21663831.2024.2305261

Fang, Y., Kim, M.-K., Zhang, Y., Duan, Z., Yuan, Q., & Suhr, J. (2025). Enhanced strength-ductility synergy in additively manufactured micro-laminated duplex stainless steel matrix composites with multiple heterogeneous structures. *Additive Manufacturing*, *98*, 104647. https://doi.org/10.1016/j.addma.2025.104647

Fang, Y., Kim, M.-K., Zhang, Y., Kim, T., No, J., & Suhr, J. (2023). A new grain refinement route for duplex stainless steels: Micro-duplex stainless steel matrix composites processed by laser powder bed fusion. *Materials Science and Engineering: A*, *881*, 145351. https://doi.org/10.1016/j.msea.2023.145351

Francis, R., & Byrne, G. (2021). Duplex Stainless Steels—Alloys for the 21st Century. *Metals*, *11*(5), 836. https://doi.org/10.3390/met11050836

Han, Y., Liu, Z.-H., Wu, C.-B., Zhao, Y., Zu, G.-Q., Zhu, W.-W., & Ran, X. (2023). A short review on the role of alloying elements in duplex stainless steels. *Tungsten*, *5*(4), 419–439. https://doi.org/10.1007/s42864-022-00168-z

Jiang, D., Gao, X., Zhu, Y., Hutchinson, C., & Huang, A. (2022). In-situ duplex structure formation and high tensile strength of super duplex stainless steel produced by directed laser deposition. *Materials Science and Engineering: A*, *833*, 142557. https://doi.org/10.1016/j.msea.2021.142557

Li, B., Han, C., Viveganantha n, P., Kripalani, D. R., Tian, Y., Bartolo, P. J. D. S., & Zhou, K. (2022). Refined microstructure and ultrahigh mechanical strength of (TiN + TiB)/ti composites in situ synthesized via laser powder bed fusion. *Additive Manufacturing Letters*, *3*, 100082. https://doi.org/10.1016/j.addlet.2022.100082

Li, B., Zheng, H., Han, C., & Zhou, K. (2021). Nanotwins-containing microstructure and superior mechanical strength of a cu-9Al-5Fe-5Ni alloy additively manufactured by laser metal deposition. *Additive Manufacturing*, *39*, 101825. https://doi.org/10.1016/j.addma.2020.101825

Liu, Y., Shi, J., & Wang, Y. (2023). Evolution, Control, and Mitigation of Residual Stresses in Additively Manufactured Metallic Materials: A Review. *Advanced Engineering Materials*, *25*(22), 2300489. https://doi.org/10.1002/adem.202300489

Salvetr, P., Školáková, A., Melzer, D., Brázda, M., Duchon, J., Drahokoupil, J., Svora, P., Msallamová, Š., & Novák, P. (2022). Characterization of super duplex stainless steel SAF2507 deposited by directed energy deposition. *Materials Science and Engineering: A*, *857*, 144084. https://doi.org/10.1016/j.msea.2022.144084

Tao, Y., Lin, L., Ren, X., Wang, X., Cao, X., Ye, Y., Zhang, E., Gu, H., & Dai, Z. (2025). Duplex γ/α-phase evolution of biocompatible high-nitrogen stainless steel in additive manufacturing. *Journal of Materials Research and Technology*, *38*, 3199–3207. https://doi.org/10.1016/j.jmrt.2025.08.074

Wang, G., Zou, Y., Qiao, C., Shen, P., Wu, Z., Li, H., & Li, Y. (2025). Influence of selective laser melting process parameters on the microstructure, corrosion resistance, and mechanical properties of 2205 duplex stainless steel. *Journal of Materials Research and Technology*, *38*, 1825–1841. https://doi.org/10.1016/j.jmrt.2025.08.043

Wang, Y., Xu, L., Han, Y., Zhao, L., Li, H., Hao, K., & Ren, W. (2023). Super duplex stainless steel with balance ratio produced by laser directed energy deposition (L-DED). *Journal of Manufacturing Processes*, *105*, 213–218. https://doi.org/10.1016/j.jmapro.2023.09.023

Wu, K., Shen, C., Xu, P., Xin, J., Ding, Y., Wang, L., Zhou, W., Ruan, G., Zhang, Y., Li, F., Chen, M.-T., & Hua, X. (2024). Revealing the evolution of microstructure and mechanical properties with deposition energy and shielding gas to achieve phase-balanced directed energy deposition of 2205 duplex stainless steel. *Materials Science and Engineering: A*, *915*, 147197. https://doi.org/10.1016/j.msea.2024.147197

Zhao, W., Xiang, H., Yu, R., & Mou, G. (2023). Effects of laser scanning speed on the microstructure and mechanical properties of 2205 duplex stainless steel fabricated by selective laser melting. *Journal of Manufacturing Processes*, *94*, 1–9. https://doi.org/10.1016/j.jmapro.2023.03.068